Thermochimica Acta, 227 (1993) 9–18
Elsevier Science Publishers B.V., Amsterdam

Thermal analysis of plasma-sprayed thermal barrier coatings [1]

A. Tomasi [a,*], P. Scardi [b], L. Lutterotti [b] and P.G. Orsini [b]

[a] *Istituto per la Ricerca Scientifica e Tecnologica, 38050 Povo (TN), Italy*
[b] *Dipartimento di Ingegneria dei Materiali, Università di Trento, 38050 Mesiano (TN), Italy*

(Received 25 January 1993; accepted 15 February 1993)

Abstract

A DSC/TGA and XRD study on the thermal stability of yttria-stabilized zirconia TBC (thermal barrier coatings) obtained by atmosphere- and temperature-controlled plasma spray, was carried out. As-sprayed zirconica coatings were under-stoichiometric and highly disordered. The thermal analysis showed that several endo- and exothermic phenomena take place on heating the ceramic. TGA clearly showed weight gains associated with the oxygen recovery, whereas DSC also detected the structural relaxation and transformations found by XRD. The activation energies, reaction order and mechanism are also discussed.

INTRODUCTION

Thermal barrier coatings (TBC) produced by plasma spray (PS) are widely used to improve the properties of several engine components working in the extreme conditions of high temperatures. The most noteworthy applications are in gas turbines, but conventional engines, such as diesels, also benefit from TBC spraying onto piston heads, valves and other mechanical parts [1].

Among the possible ceramic materials, stabilized zirconia is ideally suited to TBC applications because of its superior thermomechanical properties. As well as its high durability and refractory nature, the thermal expansion coefficients of zirconia materials ($7–13 \times 10^{-6}\ K^{-1}$, depending on the stabilizer type and content [2–4]) are very close to those of steels and many metal alloys. However, to be effective as a coating material, zirconia must be stable over wide temperature range, from room temperature (RT) up to above 1000°C. Pure zirconia has three polymorphs at normal pres-

* Corresponding author.

[1] Presented at the 14th National Conference on Calorimetry and Thermal Analysis, Udine, 13–17 December 1992.

sure: monoclinic (RT), tetragonal ($1170 < T < 2370$°C) and cubic ($T >$ 2370°C), before the melting point (2680°C). To retain a single phase over a more or less wide temperature range, stabilizing oxides such as yttria, ceria, calcia or magnesia, can be alloyed to pure zirconia. Typical compositions for TBC are 8 wt.% Y_2O_3 (tetragonal) or 20 wt.% Y_2O_3 (cubic).

In addition to the effect of the composition, the TBC microstructure and properties are strongly influenced by several process parameters. Due to the high temperature involved, the plasma is a highly reducing environment. As was shown for CeO_2-stabilized zirconia, the degree of oxidation of the stabilizer changed noticeably after the spraying [5]. Working on plasma composition, it has also been shown that zirconium suboxides can be formed during the spraying of Y_2O_3-stabilized zirconia powder [6]. All these effects introduce oxygen vacancies that change the phase composition of the coatings.

In the present work, the thermal evolution of 8 wt.%-Y_2O_3-stabilized zirconia coatings ($Zr_{0.913}Y_{0.087}O_{1.957}$) produced by ATCS (atmosphere- and temperature-controlled spraying), was followed. The results of differential scanning calorimetry (DSC) and thermal gravimetry (TG) were combined with structural information from X-ray diffractometry (XRD) in order to study the thermal stability of the coatings.

EXPERIMENTAL

Plasma spray coatings were produced using an SNMI (Societé Nouvelle de Metallization Industriel) plasma set in the ATCS mode. Details of the preparation will be reported elsewhere [7]. Metco 204NS powder [8] (8 wt%-Y_2O_3-stabilized zirconia) was used as raw material for the spraying.

The thermal analysis was carried out using a Perkin-Elmer Model 7 TGA/DSC apparatus; the samples for the analysis were detached mechanically from the ceramic coating. All reported curves were corrected using a second run as a baseline.

XRD analysis was conducted using a Rigaku diffractometer, equipped with a graphite monochromator in the diffracted beam, using Cu Kα radiation produced at 40 kV and 30 mA. Each 0.05° step was counted for 12 s in the range 20–150°.

The samples analyzed were: as-sprayed coating (TQ), samples heat-treated for 5 h at 200°C (A), and samples heat-treated for the same time at 300 (B), 400 (C) and 500°C (D), always on the same sample.

A method recently devised by some of the authors, based on the Rietveld algorithm, was employed for XRD data-processing [9]. Through this method, a very precise quantitative analysis of the zirconia polymorphs can be carried out, together with the simultaneous refinement of lattice parameters, crystallite size and microstrain, also considering the presence of preferred orientations [10].

RESULTS

The as-sprayed coatings were dark gray, with the typical lamellar microstructure of PS ceramic coatings, as shown in Fig. 1. The columnar structure inside each lamella is clearly visible. As found in previous EPR and XPS studies, the dark color is associated with the lack of oxygen, i.e. the presence of zirconium suboxides [6].

In order to study the thermal stability, the oxygen vacancies introduced during the spraying and the mechanism of the reaction, TG analyses were carried out using non-isothermal methods. The curves reported in Fig. 2, obtained with heating rates of 2, 5, 10, 20 and 30°C min^{-1}, clearly show two different weight gains. The first, at low temperature, is sharp, at around 100°C, and yields a weight gain of 0.08%. The second smaller weight gain (0.04%) is distributed over a large temperature range and is completed at 600°C.

In order to study the reaction order and mechanism, the Satava method was followed [11]. For each heating rate, the temperature was correlated with the reacted phase fractions a obtained from the DTG peak. Several equations $g(a)$ related to four different processes — diffusion (D), phase boundary reaction (R), nucleation and growth (N), and power law (P) — were tested. As an example of the data processing, Fig. 3 shows the curves obtained from the DTG data at 10°C min^{-1} by plotting $\log g(a)$ versus $1/T_a$.

Table 1 reports the mean linear correlation coefficients r for the different heating rates for the various models tested. A straight line ($r = 1$) should result for the data fitted by the correct mechanism. The best agreement was found for the R3 function. The kinetic study was carried out only for the

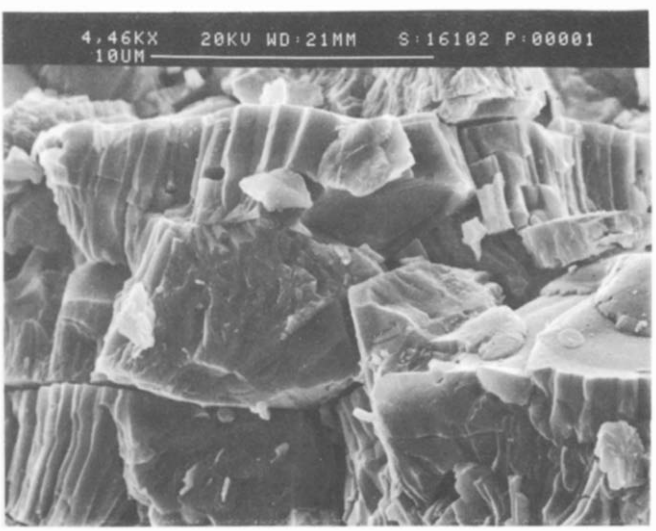

Fig. 1. Fracture surface on 8 wt.%-Y_2O_3-stabilized zirconia TBC.

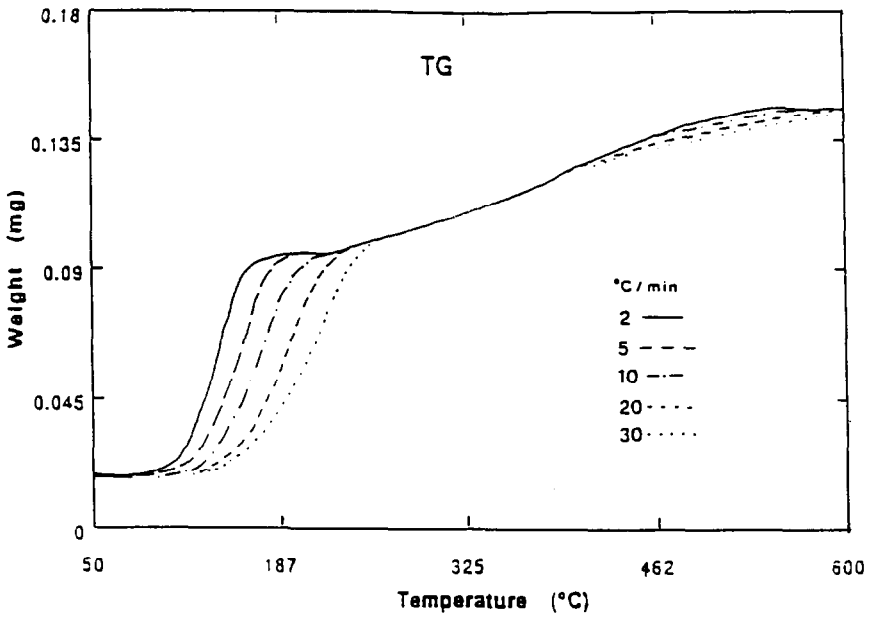

Fig. 2. TGA curves obtained at 2, 5, 10, 20 and 30°C min^{-1}.

first weight gain, because the DTG peak was only clear in this temperature range.

Using the Satava method, it is also possible to calculate the activation energy of the process from the slope of the straight line. The value obtained, 16.0 kcal mol^{-1}, was compared to that given by the Ozawa method [12], which considers only the peak temperature; the value obtained, 17.0 kcal mol^{-1}, is in agreement with that obtained by Satava's method. This demonstrates the effectiveness of the method used and the correctness of the mechanism found: phase boundary reaction with spherical symmetry.

DSC in air, performed at the same heating rates as TGA (Fig. 4) showed a well-shaped exothermic peak that was first attributed to the oxidation. A less visible broad peak was present at higher temperature for heating rates greater than 5°C min^{-1}. A broad endothermic effect was found above 300°C. This peak was obvious at low rates; high rate scans showed only part of the peak, at very high temperature. The same kinetic study as for TGA was carried out for the first DSC peak; the results are reported in Table 1. The activation energy was 18.5 and 19.9 kcal mol^{-1} using Satava's and Ozawa's methods, respectively.

Figure 5 shows the experimental and modeled XRD patterns for samples TQ (as-sprayed) and B (heat treated). The main visible difference is in the monoclinic (m) phase content. The as-sprayed coating has a very low m-phase content whereas, after heat treatment, the percentage

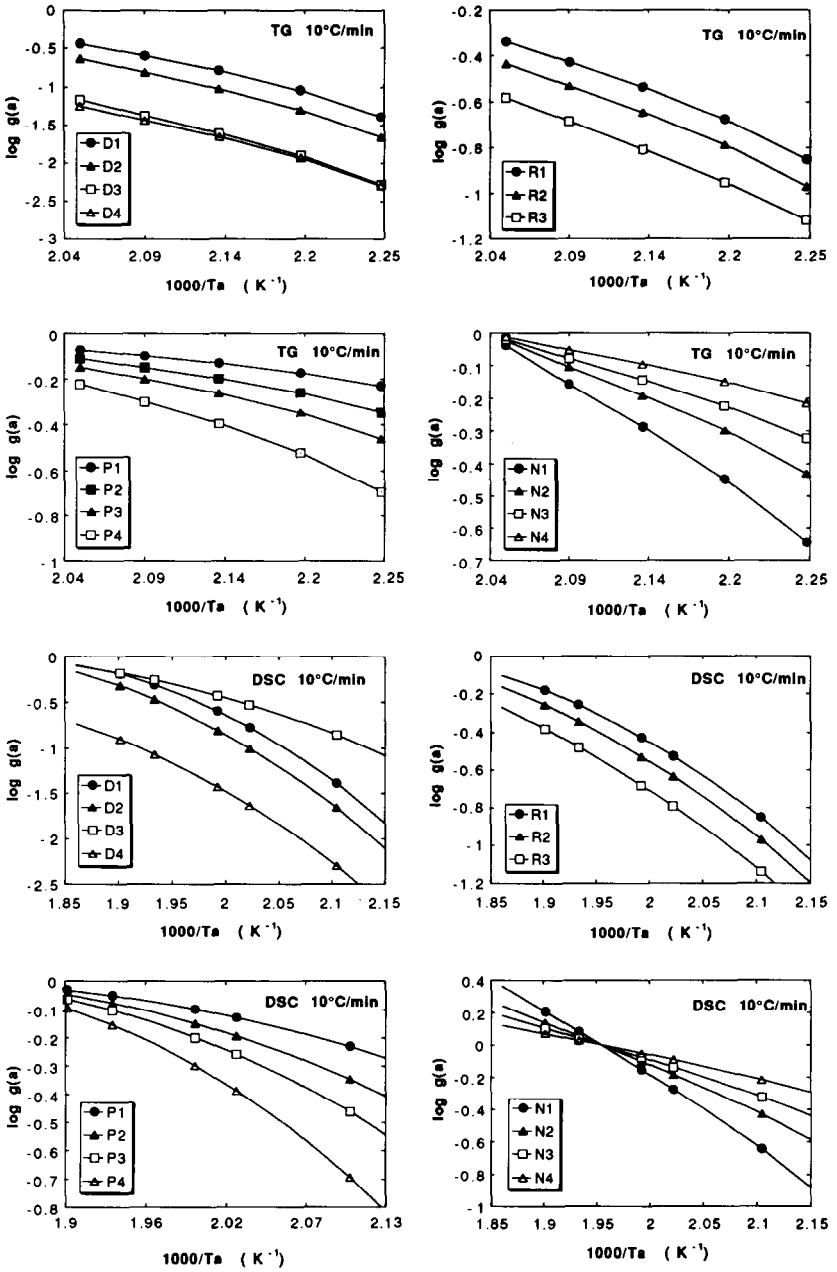

Fig. 3. Data fitting obtained from TG and DSC curves at 10°C min^{-1} for different processes, following Stava's method.

TABLE 1

Mean linear correlation coefficients r for the different heating rates for the various functions tested

	$g(a)$	r(TG)	r(DSC)
D1	a^2	0.9633	0·9784
D2	$(1-a)[\ln(1-a)]+a$	0.9756	0.9864
D3	$[1-(1-a)^{1/3})]^2$	0.9858	0.9885
D4	$(1-2a/3)-(1-a)^{(2/3)}$	0.9802	0.9893
R1	$1-(1-a)^{(2/3)}$	0.9773	0.9870
R2	$1-(1-a)^{(1/2)}$	0.9830	0.9910
R3	$1-(1-a)^{(1/3)}$	0.9988	0.9932
P1	$a^{(1/3)}$	0.9660	0.9772
P2	$a^{(1/2)}$	0.9661	0.9772
P3	$a^{(2/3)}$	0.9661	0.9772
P4	a	0.9661	0.9772
N1	$[-\ln(1-a)]$	0.9898	0.9988
N2	$[-\ln(1-a)]^{(2/3)}$	0.9898	0.9986
N3	$[-\ln(1-a)]^{(1/2)}$	0.9897	0.9980
N4	$[-\ln(1-a)]^{(1/3)}$	0.9897	0.9980

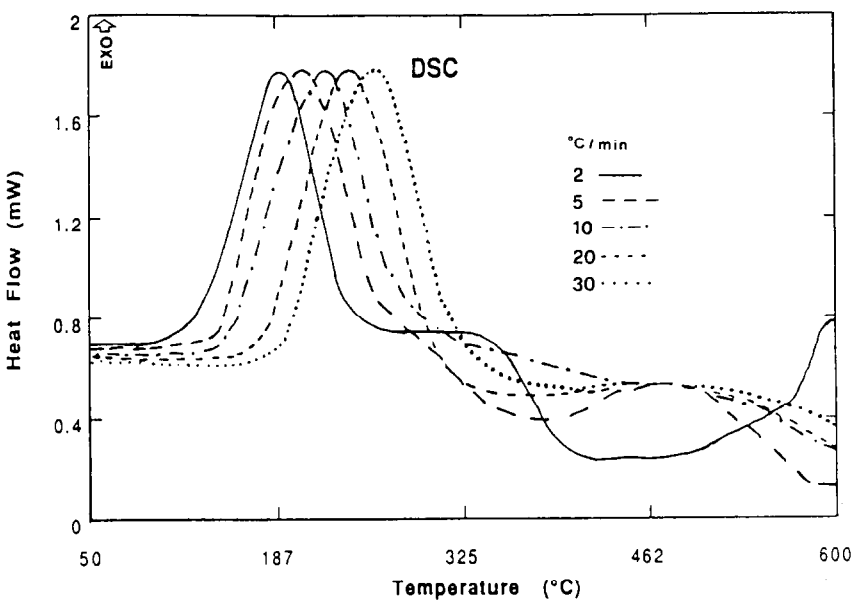

Fig. 4. DSC curves obtained at 2, 5, 10, 20 and 30°C min^{-1}.

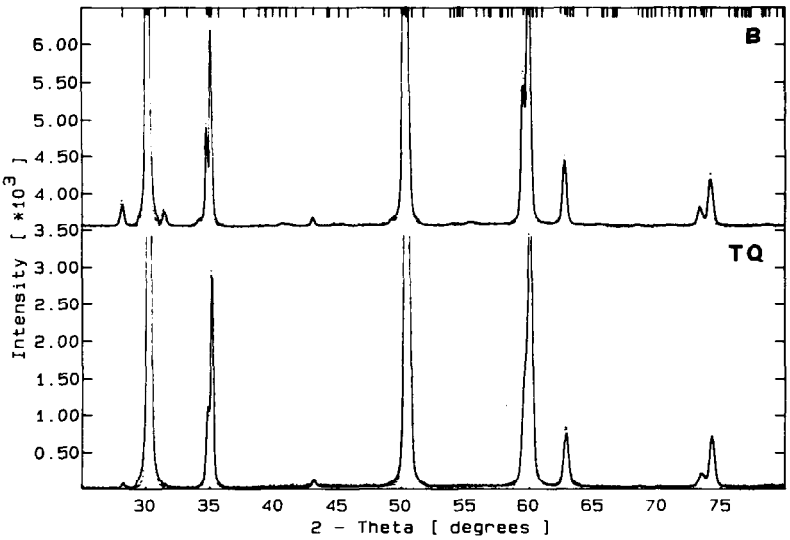

Fig. 5. Experimental (· · ·) and modeled (—) XRD data for as-sprayed (TQ) and thermally treated (B) coatings.

increased. In addition, the TQ profiles are noticeably broader than those of the heat-treated samples. The results of all the analyses are summarized in Fig. 6, which reports the m-phase percentage, a/c (tetragonality), t-phase cell volume, crystallite size and microstrain as a function of the thermal treatment.

DISCUSSION

The spraying was carried out in argon atmosphere, using a liquid argon jet as the cooling system. Under these conditions, the material was strongly reduced in the high-temperature plasma and the droplets arriving at the target, whose temperature was kept at 140°C by the cooling jet, were quenched. For these reasons, zirconium oxide is expected to be under-stochiometric. The lack of oxygen, i.e. the presence of anionic vacancies, enhances the stabilizing action of Y_2O_3, which is also based on the introduction of vacancies [13]. Thus, a t-phase excess is expected, because part of the pure zirconia present in the raw material [14] and the fraction of ceramic with insufficient stabilizer content, can be retained in the tetragonal form, stabilized by vacancies, after the spraying.

DSC and TGA confirmed the XPS and EPR observation [6] regarding the presence of zirconium suboxides in the as-sprayed coatings. In fact, the TGA weight gain and the DSC exothermic peak are clearly due to the oxidation of the coating. After the thermal treatments, the color of samples turned to white, suggesting a recovery of a stable degree of oxidation. If we consider the weight gain (0.12 wt.%) as due to an oxidation, the

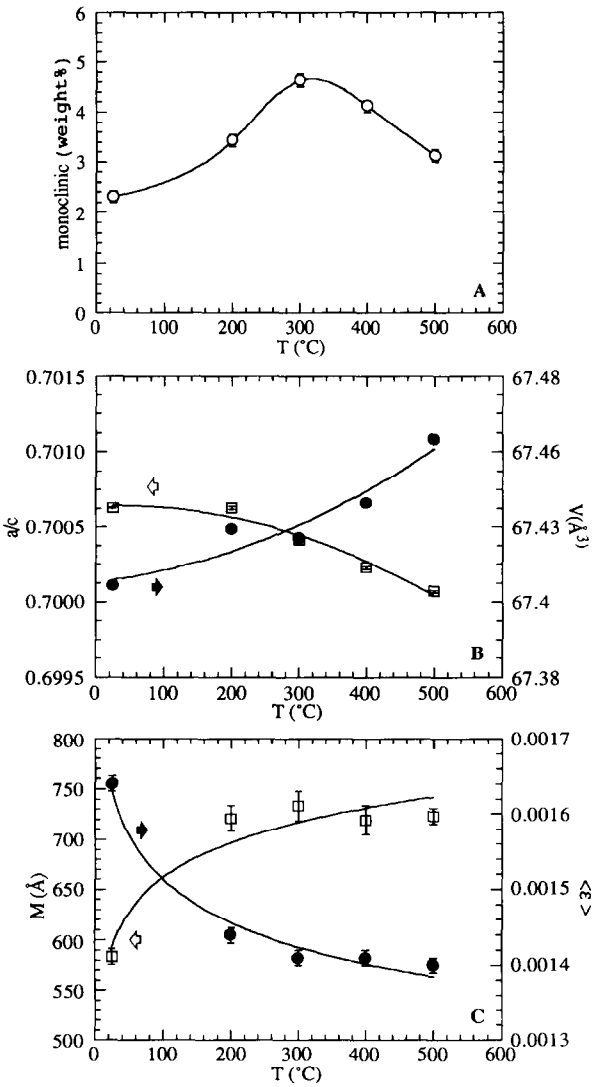

Fig. 6. Results of XRD total-pattern analysis after several thermal treatments: A, monoclinic phase percentage; B, tetragonality (a/c) and t-phase cell volume; C, crystallite size and microstrain.

mean stoichiometry of the material changed from $Zr_{0.913}Y_{0.087}O_{1.947}$ to $Zr_{0.913}Y_{0.087}O_{1.857}$ after each thermal analysis.

The kinetic study of the TGA data (see Table 1) indicated that a phase boundary reaction occurred. Thus, the two-step TGA weight gain of Fig. 2 can be explained by considering that the oxidation first takes place at the surface, through open porosity and grain boundaries, and then, slowly and at higher temperature, through bulk diffusion. In any case, the maximum rate of weight gain always occurred at temperatures lower than the DSC

peak, probably because of a kinetic effect; in fact, the oxygen was initially absorbed at the surface and then it needed to diffuse through the first-formed oxide before the oxidation could be completed.

It is worth noting that the activation energy found by TGA is notably smaller than that obtained by DSC. Moreover, as reported in Table 1, the DSC kinetic study indicates a first-order reaction with a nucleation and growth mechanism, whereas TGA suggests a phase boundary reaction with spherical symmetry. This discrepancy can be explained from the XRD results. In fact, as can be seen in Fig. 6, in the range of the large exothermic effect, an m-phase increase occurs, together with a decrease in microstrain decrease and an increase in crystallite effective size. A positive (5%) volume change is associated with the t- to m-phase transformation, resulting in an endothermic reaction; the microstrain reduction is probably due to a structural relaxation that also creates the size of the coherently diffracting domains, giving an exothermic effect. Thus the DSC signal can be considered as the sum of all these phenomena; for this reason the reaction mechanism and the activation energy obtained by DSC are different from those obtained by TGA because the DSC signal is influenced by several effects.

Because TGA measures only the oxygen recovery, the activation energy is relative to this single effect and it represents the occurrence of a surface reaction. However, the reaction order and mechanism obtained from DSC are linked with the reaction-controlling stage. All phase structural transformations taking place on heating (t- to m-phase and t-phase expansion) are triggered by the oxidation. Thus, it can be assumed that these reactions are slower because they probably follow the oxygen recovery and are balanced by matrix constraints. Following this hypothesis, the reaction mechanism indicated by DSC can be due to the structural transformations that follow a nucleation and growth mechanism [15]. Further work will be necessary to clarify this point.

The DSC data exhibit a large endothermic effect between 350 and 550°C, which is clearly visible at low heating rate. At first sight this seems inexplicable if we consider the second weight gain in the same temperature range. Even in this case, this misleading evidence is due to the overlapping of different phenomena. As shown in Fig. 6, in addition to the phase transformation, the t-phase is subjected to a considerable volume change, with an increase in tetragonality. This effect, which is more apparent at high temperature, is due to the continuous oxygen recovery of the ceramic.

Finally, the slight decrease in the m-phase percentage observed after the treatments at 400 and 500°C, is probably due to the beginning of the m- to t-phase transformation. In fact, the transformation temperature is lowered by the presence of stabilizer and, after the transformation, the t-phase can be retained by structural constraints. Such hysteresis effects are well known in zirconia materials [16].

CONCLUSIONS

Thermal barrier coatings of Y_2O_3-stabilized zirconia produced by plasma spraying in Ar atmosphere and liquid Ar cooling, tested by thermal analysis, exhibit a considerable thermal instability associated with the presence of oxygen vacancies and microstructural disorder inside the ceramic top coat. While TGA proved to be effective in detecting a lack of oxygen, and in determining the activation energy and the reaction mechanism of the oxidation, DSC patterns are influenced by several effects, both endo- and exothermic, that complicate their interpretation. Using the information obtained by the total pattern-fitting of XRD data, it was possible to distinguish several phenomena taking place on heating the coatings. Apart from the t–m phase change associated with the oxidation, a remarkable increase in t-phase cell volume and tetragonality was found. As-sprayed coatings are highly defective; as shown by XRD and DSC, a structural relaxation occurred after heat treatment.

ACKNOWLEDGMENTS

The authors thank Dr. E. Galvanetto who supplied the samples and Mr. S. Setti for technical assistance during XRD measurements. This work was partly supported by CNR-P.F. Matriali Speciali per Tecnologie Avanzate.

REFERENCES

1 A. Bennet, Mater. Sci. Technol., 2 (1986) 257.
2 J.R. Brandon and R. Taylor, Surf. Coat. Technol., 39 (1989) 143.
3 S. Rangaswamy, S. Safai and H. Herman, in T.A. Hahn (Ed.), Thermal Expansion 8, Plenum Press, New York, 1984, p. 93.
4 P. Scardi, R. Di Maggio, L. Lutterotti and P. Maistrelli, J. Am. Ceram. Soc., 75 (1992) 2828.
5 R. Dal Maschio, P. Scardi, L. Lutterotti and G.M. Ingo, J. Mater. Sci., 27 (1992) 5591.
6 P.G. Orsini, R. Dal Maschio, F. Marino and P. Scardi, in S. Meriani and C. Palmonari (Eds.), Zirconia 88, Bologna, Elsevier, Amsterdam, 1989, p. 229.
7 P. Scardi, L. Lutterotti and E. Galvanetto. Surf. Coat. Technol., submitted.
8 METCO, Division of Perkin-Elmer, Metco 204NS, Cat. P204NS-10.
9 L. Lutterotti, P. Scardi and P. Maistrelli, J. Appl. Crystallogr., 25 (1992) 459.
10 L. Lutterotti and P. Scardi, J. Appl. Crystallogr., 23 (1990) 246.
11 V. Satava, Thermochim. Acta, 2 (1971) 423.
12 T. Osawa, J. Therm. Anal., 2 (1970) 301.
13 P. Adelbert and J.P. Traverse, J. Am. Ceram. Soc., 68 (1985) 34.
14 P.G. Orsini, P. Scardi and L. Lutterotti, Mater. Eng., submitted.
15 A.H. Heuer, M. Ruhle, Acta Metall., 33 (1985) 2101.
16 C.A. Anderson and T.K. Gupta, in A. H. Heuer and L.W. Hobbs (Eds.), Advances in Ceramics—Science and Technology of Zirconia, Vol. 3, The American Ceramic Society, Columbus, Ohio, 1981, p. 184.